Journal of Solid State Chemistry 267 (2018) 98–105

Contents lists available at ScienceDirect

Journal of Solid State Chemistry

journal homepage: www.elsevier.com/locate/jssc

Influence of carbonate and nickel(II) concentration on the synthesis of calcium phosphates

J.R. Guerra-López[a,*], J.A. Güida[a,b,c], A.E. Bianchi[c,d], G. Punte[d]

[a] Departamento de Ciencias Básicas, Universidad Nacional de Luján, rutas 5 y 7 Luján, CC 6700, Argentina
[b] CEQUINOR (CONICET-CCT La Plata), Departamento de Química, Facultad de Ciencias Exactas, Universidad Nacional de la Plata, Boulevard 120 No 1465, 1900 La Plata, Argentina
[c] Departamento de Ciencias Básicas, Facultad de Ingeniería, Universidad Nacional de la Plata, 115 y 49, 1900 La Plata, Argentina
[d] IFLP (CONICET-CCT La Plata), Departamento de Física, Facultad de Ciencias Exactas, Universidad Nacional de la Plata, 115 y 49, 1900 La Plata, Argentina

ARTICLE INFO

Keywords:
Urinary calculi
Brushite
Carbonate apatites
Infrared spectroscopy
Powder x ray diffraction

ABSTRACT

Two sets of Ni-substituted calcium phosphate were synthesized by precipitation method at pH = 7 and at two different concentrations of ion carbonate (CO_3^{2-}) in solution and Ni(II) concentrations lower than 15%. The produced solids were characterized by chemical analysis, infrared spectroscopy, x-ray powder diffraction and scanning electron microscopy. The solid samples obtained at low concentration of CO_3^{2-} (5%) and Ni(II) concentrations 5%, 10% and 15% were synthesized at 25 and 37 °C. All solids showed the presence of a stable and crystalline brushite ($CaHPO_4{\cdot}2H_2O$). The samples synthesized in presence of high levels of carbonate (50%) and Ni(II) concentration 5% at 25, 37 and 100 °C vary with temperature. Those obtained at the lower temperatures (25 and 37 °C) showed coexistence of two phases: a crystalline $CaCO_3$ and carbonate apatite with low crystallinity. At 100 °C, only carbonate apatite could be recognized. Data supported the carbonate substitution by OH^- (position A) and PO_4^{3-} (position B) in the hydroxyapatite structure. The comparison of the chemical analysis results of both systems studied (Ni,Ca) apatite and (Ni,Ca) carbonate apatite evidences a rise of Ni(II) incorporation in the apatite lattice, with simultaneous inclusion of CO_3^{2-} and temperature increase. The obtained results suggest that brushite kidney stones development may be induced by the presence of traces of Ni(II) and simultaneous decrease of carbonate levels in the biological fluids.

1. Introduction

The increment of urolithiasis detection in the developed countries during the last decades has triggered a great number of research efforts and statistical analysis trying to find ways to improve the management of this health condition [1,2]. Calcium oxalate renal stones incidence has raised, being the more frequently identify (85%). This prevalence seems to be increasing and has been attributed to changes in the quality of food consumed, which is abounding in proteins, salt and carbonates [3–5]. Besides, more than 50% of those stones are a combination of calcium oxalate with variable amounts of brushite ($CaHPO_4{\cdot}2H_2O$, DCPD) and calcium hydroxyapatite ($Ca_{10}(PO_4)_6(OH)_2$, CaHap) as a nucleus [1–3]. The latter phases have been associated with first stages of mineral stone formation. Calcium phosphates (Ca-P) salts presence has been regarded as a key factor in assessing the risk of stone formation [1,6]. This model arises from evidences that, at urine pH values from 5 to 7, the precipitation of Ca-P like amorphous calcium phosphate, brushite and octacalcium phosphate [7,8], take place prior to spontaneous transformation to apatite at high pH [9]. However, going deeper into stone morpho-constitutional analysis by means of techniques like X-ray powder diffraction (XRPD), infrared spectroscopy (FTIR), micro–computed tomography (Micro-CT) and scanning electron microscopy (SEM), it has been found that information on crystalline phases of the same chemical species (like calcium oxalate mono or dihydrate) may imply different etiopathogenic conditions and the nucleation process could be related to another mechanism than the factors responsible for the subsequent stone growth [10]. All these considerations evidence the importance of accurate stone analysis including stone morphology, chemical composition and crystalline phases, as the location of these phases within the stone. Even getting a good knowledge about stone microstructure [10], which helps to determine some causes of stone retention while small in size, the process will not be fully understood as

* Correspondence to: Departamento de Ciencias Básicas, Universidad Nacional de Luján, rutas 5 y 7 Luján, CC 6700, Argentina.
E-mail addresses: joseguerralopez1@gmail.com (J.R. Guerra-López), guida@quimica.unlp.edu.ar (J.A. Güida), bianchi@fisica.unlp.edu.ar (A.E. Bianchi), punte@fisica.unlp.edu.ar (G. Punte).

https://doi.org/10.1016/j.jssc.2018.08.010
Received 4 June 2018; Received in revised form 19 July 2018; Accepted 12 August 2018
Available online 14 August 2018
0022-4596/

those causes would not be unique [11]. Therefore, different approaches have been tried, many of them referred to brushite stone formation, as they are difficult to deal with and highly recurrent. Some studies mimic stone mineralization process in diverse environments which may favor or impair growth conditions, others address the influence of foreign metals on Ca-P salts formation [12–15].

In previous work, we had studied the influence of different metal ions on calcium phosphate crystallization and their incidence on biological mineralizations [13,16]. From those studies, we found out that under the synthesis conditions (neutral pH and two different temperatures: 25 and 37 °C) only brushite phase is formed when up to a 15% of Ni(II) is included in phosphate synthesis. For larger Ni(II) concentration in solution, other phases are formed. The results suggested that brushite kidney stones may develop as a consequence of the presence of traces of Ni(II) in biological fluids. Besides, we had found that Ni(II) traces may induce amorphous calcium phosphate formation, which also facilitates calcium oxalate nucleation [16,17].

In this work, we try to add to the knowledge of brushite formation and stabilization in controlled conditions. The effects of Ni(II) on the transformation of brushite to CaHap when different proportions of CO_3^{2-} ions are simultaneously present in the mother solution in different proportions will be explored. The systems, named below "high concentration carbonate", reproduce the urinary fluid observed values [13,14], which are partially due to the normal bone regeneration process. Solid products obtained were analyzed by atomic absorption spectroscopy (A.A.) and characterized by XRPD, SEM and FTIR. The obtained results are presented below. They are compared with data achieved in previous studies [16,18] and in the literature [19–25]. Possible relation of the produced samples with the development of kidney stones is also discussed.

2. Experimental

To make clear the optimal synthetic conditions necessaries to obtain hydroxyapatite and brushite from solutions, both processes are described below along with the synthetic process employed to produce the materials to study in the present work.

2.1. Calcium hydroxyapatite synthesis

CaHap was prepared introducing slight modifications to Hakey y Newesely's method [13]. Two solutions 0.1 M of hydrogen ammonium phosphate (Merck, pro analysis) and acetate (or nitrate) of the metals were prepared. These solutions were added simultaneously at the same rate to a constantly stirred solution containing ammonium acetate 0.1 M (Merck, Pro Analysis) at a temperature (T) of 98 °C [13,17]. The addition rates were fixed to a value that allows to keep pH = 7. The precipitate was stored for 24 h in contact with their solution. Then, it was filtered, washed with distilled water and dried at T = 80–100 °C. If crystallinity improvement was necessary, drying at T = 200 °C for several hours was performed.

2.2. Brushite synthesis

Brushite was prepared by the method of Tovborg-Jensen and Rathlev [26]. A solution containing 0.5 mol of Na_2HPO_4 $8H_2O$ (BDH, Pro Analysis) and 0.4 mol of KH_2PO_4 (Merck, Pro Analysis) per liter of water and a solution containing 0,5 mol of $CaCl_2{\cdot}6H_2O$ (Merck, Pro Analysis), were prepared. These solutions were added simultaneously at the same rate to a constantly stirred solution containing KH_2PO_4 0.1 M at 25 °C. The addition rates were maintained in order to keep the pH at 4.8. The solid precipitate was filtered, washed with H_3PO_4 (85% J. T. Baker, Pro Analysis) 0.05% and dried at 60 °C [16].

2.3. Calcium phosphate synthesis in presence of Ni(II) cations and CO_3^{2-} anions

The preparation method was adapted from the procedure employed to synthesize hydroxyapatite doped with zinc (Ca,Zn)Hap [27]. The phosphates were prepared by dropwise addition of two solutions 0.2 M, (one of calcium and nickel acetate (Fluka, Pro Analysis)) and the other of ammonium phosphates (BDH, Pro Analysis) to a stirred solution of ammonium acetate (Merck, Pro Analysis). The experimental conditions of reaction were: temperature 25 °C or 37 °C and pH 7. Since, in the course of the synthesis the amount of $[H_3^+O]$ in solution changes; NH_3 (30% Merck, Pro Analysis) or acetic acid (99% Merck, Pro Analysis) 0.1 M were added to keep the pH of the solutions constant. Measurements of pH were made by means of an MV 870 digital pH meter and using a combined glass electrode. The electrode was calibrated at 25 °C with a buffer prepared according to the National Bureau of Standards [28].

2.3.1. Low concentration of CO_3^{2-} (5%)

Phosphates were prepared by dropwise addition of two solutions 0.2 M, one of calcium and nickel acetate and other of ammonium phosphate and ammonium carbonate (J.T. Baker, Pro Analysis), to a stirred solution of ammonium acetate at pH 7 and at 25 and 37 °C. The composition of the solution was varied in steps, from pure calcium acetate to 15% of Ni and 85% of calcium acetate. The upper range of [Ni/Ca] ratio in the solution was selected based on a previous study, which showed that nickel concentrations 20% and over induce the formation of mixed phases [16]. The solid samples obtained were named by the nickel and carbonates symbols, followed by an l (from low) and a number, n, which indicates the nickel concentration in the solution expressed as at%, ($NiCO_3ln$).

2.3.2. High concentration of CO_3^{2-} (50%)

In this case, the preparation method was adapted from the results obtained in the synthesis described above. The composition of the solution employed was 5% of nickel acetate and 95% of calcium acetate with 50% of ammonium phosphate and 50% ammonium carbonate. The synthesis procedure was performed at three different temperatures: 25, 37 and 100 °C.

The carbonate/phosphate relation employed was chosen to take into account the results obtained by LeGeros et al. [19,29]. The solid samples were named by the nickel and carbonates symbols followed by an h (from high) and a number, n, which indicates the nickel concentration in the solution expressed as at%, ($NiCO_3hn$).

During the synthesis, either at low or high carbonate concentrations, the amount of $[H_3^+O]$ increases, and, to keep the pH of the solutions constant, NH_3 or acetic acid 1 M was added at the selected temperature. The solid samples obtained were named as described above adding the number m (as a subscript), which indicates the temperature of the reaction, ($NiCO_3hn_m$).

2.4. Samples characterization

All the samples were characterized by XRPD, FTIR and A.A.; SEM images of selected samples were also obtained.

Sample preparation for FTIR spectra was described in reference 27. The FTIR spectra were recorded with a Bruker 66 spectrometer in the range 4000–400 cm^{-1}, with a 4 cm^{-1} resolution. XRPD data were obtained with a Philips PW1710 powder diffractometer, provided with a diffracted beam monochromator, using Cu Kα monochromatic radiation (λ = 1.5406 Å). The 2θ range covered was from 3° to 120° with a step interval of 0.02° and a counting time of 5 s.

The composition of the products was checked by the determination of Ca, Ni, P and carbonate contents. Ca and Ni were determined by A.A. with a Perkin Elmer AAnalyst 200 at. absorption spectrometer, equipped with a graphite furnace HGA 900. Phosphorus was deter-

Table 1
Content of Ni(II) in solid phase synthesized in presence of low concentration of carbonate in solution (5%).

Initial Ni(II) in solution		Ni(II) in reaction products			
x = Ni (% in mol)[a]	Ni (% in wt)	Ni in solid (% in wt)[b]	Ni in solid (%)[c]	Ni in liquid (%)[c]	Ni in solid (Ca+Ni)/P
5	3.0	2.8 ± 0.1	94.0	6.0	1
10	5.9	5.3 ± 0.1	90.0	10.0	0.98
15	8.8	7.0 ± 0.1	80.0	20.0	0.95

[a] Initial Ni concentration before reaction, calculated by: Ni/(Ca+Ni)*100; x is related to brushite formula: $Ca_{(10-x)}Ni_xPO_4{\cdot}H_2O$.
[b] Ni concentration was quantified.
[c] Ni Percentage of expected value [(column3/column2)*100].

mined spectrophotometrically by a method developed by Portal [13]. The carbonate ion was determined by digestion and subsequent titration.

The morphological characteristics of the crystallites were analyzed from images obtained with a FEI ESEM Quanta 200 – Environmental Scanning Electron Microscope.

3. Results

3.1. Samples synthesized in presence of low concentrations of carbonate ions

3.1.1. Chemical analysis

The results of the chemical analysis of the phosphate samples synthesized in the presence of low concentration of CO_3^{2-} (5%) are summarized in Table 1. The values are very similar to those obtained for $(Ca,Ni)HPO_4{\cdot}H_2O$ samples in previous work [16]. The molar (Ca+Ni)/P ratio found in the solid was in the range of 0.97–1, thus evidencing cation vacancies in the solid. Analysis of data of Table 1 shows that nickel incorporation in the solid is almost complete from Ni5 to Ni15 (82%). It should be noted that no carbonate ions were detected in any of the solids analyzed. This behavior was attributed to the formation of brushite doped phases (see spectroscopic, diffraction and SEM results below).

3.1.2. Infrared spectra

Fig. 1 compares the infrared spectra of synthesized samples $NiCO_3l5$ and $NiCO_3l10$ at 25 °C (B and C curves) with that of brushite (A). It can be seen that small and continuous changes in bands widths and positions appeared. The increase in the intensity of the water-related bands 3500–3200, ν_1 and ν_3, 1600, $\delta(H_2O)$ and 670 cm^{-1} (waters libration)] was noticed when going from brushite to $NiCO_3l0$, evidencing an augment of the water absorption in the structure. A small shift of ν_3 water band towards low frequencies with the increase of nickel concentration was registered, as it was observed previously [16]. It is important to note that the infrared spectra for nickel doped samples do not present bands which can be associated with carbonate ions. These results evidence, in agreement with chemical analysis, that the materials contained no traces of carbonate. The FTIR spectra of samples obtained at 37 °C are not shown because no appreciable difference was observed when compared with data coming from samples obtained at 25 °C. Neither table of bands assignments nor additional discussion about the spectrum in another spectroscopic region have been included as results are coincident with those ones published previously for samples synthesized in absence of carbonate [16].

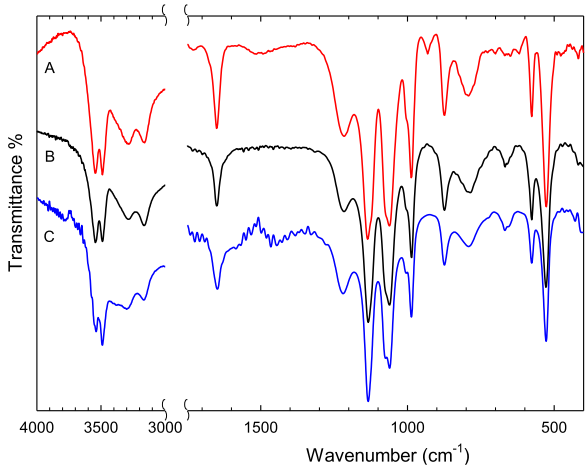

Fig. 1. Infrared spectra for the calcium phosphate phase with different nickel percent: A) brushite, B) $NiCO_3l5$ and C) $NiCO_3l10$ obtained at 25 °C.

3.1.3. X-ray diffraction results

X-ray diffraction patterns for $NiCO_3l5$ and Ni5 (the later, obtained in previous work [16] was included for comparison) are shown in Fig. 2, where Ni5 and $NiCO_3l5$ are labeled A and B, respectively. The analysis of the patterns showed that the inclusion of 5% of carbonate ions in the solution does not modify the main structural features. $NiCO_3l5$ shows brushite and traces of monetite. Going from Ni5 to $NiCO_3/5$, monetite phase percentage increase. The higher intensity line of this phase is marked with an arrow in both diffraction patterns in Fig. 2. To analyze the X-Ray data, we employed the structural models of Curry and Jones for brushite [30] and Catti et al. for monetite [31]. The Rietveld refinements using these structural models at the initial stages lead to an estimation of 85% brushite and 15% monetite with e.s.d.'s of 3% in $NiCO_3l5$.

3.1.4. SEM images

The morphological characteristics of $NiCO_3l5$ crystallites can be seen in Fig. 3. Both images show bunches of well defined crystals, which are similar to those detected in brushite samples coming from kidney stones studied by different authors [20,21].

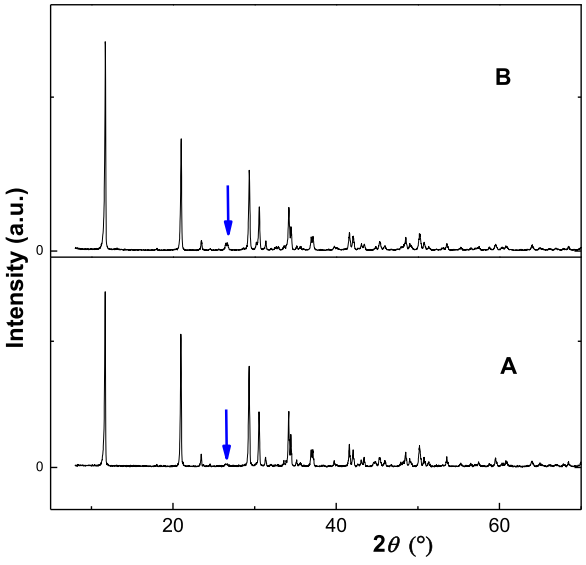

Fig. 2. XRPD patterns of samples synthesized from solutions with 5% of nickel in the following conditions: A) no carbonate anion in solution, Ni5 [16], and B) low level of carbonate anions (5%), $NiCO_3l5$.

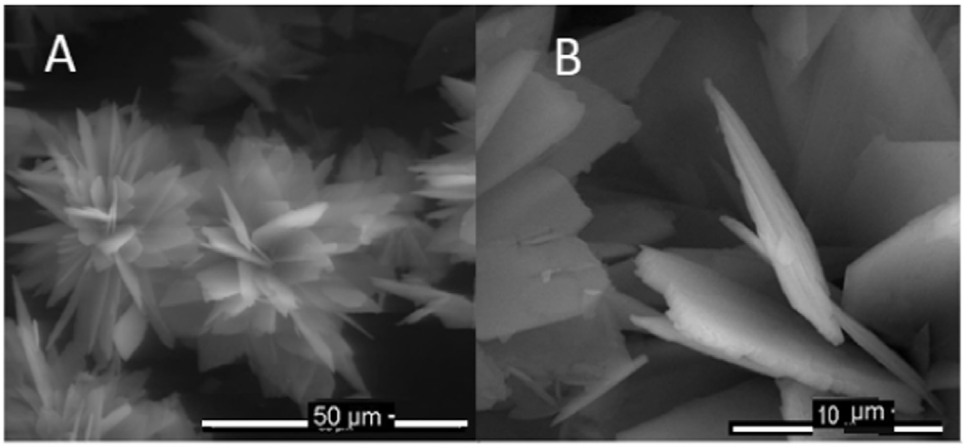

Fig. 3. SEM image of $NiCO_3h5$ crystallites. Scales: A) 50 μm; B) 10 μm.

3.2. Samples synthesized in presence of high concentrations of carbonate ions

3.2.1. Infrared spectra

The infrared spectra coming from samples obtained in presence of high concentrations of carbonate ions in solution at different temperatures, $NiCO_3h5_{25}$, $NiCO_3h5_{37}$ and $NiCO_3h5_{100}$ label C, D and E, respectively, are shown in Figs. 4 and 5. These spectra do not resemble brushite vibrational modes. Furthermore, features in the 1500–1400 cm^{-1} wavenumber region evidenced the incorporation of carbonate in the solid. The bands over 1000–900 and 600–550 cm^{-1} are typical for an apatitic phase, thus indicating the formation of a carbonate apatite phase (CO_3Ap).

For further analysis, FTIR spectra of samples obtained in this work with high concentration of carbonate ($NiCO_3h5_m$) at 25, 37 and 100 °C were compared with those of hydroxyapatite, CaHap, and label A in Fig. 5 [18] and of Ni(II) doped CaHap (Ca,Ni)Hap (produced with 5% of nickel [18]) and label B in Fig. 5. Bands assignments are gathered in Table 2. In the later, the A.A. results for Ni % in solid are also included.

In Fig. 5, a selected frequency region (1800–500 cm^{-1}) is shown where the bands correspondent to ν_1, ν_3 and ν_4 phosphate modes; ν_2 and ν_3 from carbonate modes and $\nu_L(OH^-)$ are observed. The CaHap spectrum (Fig. 5A) displays the characteristic features observed for synthetic hydroxyapatite [12,13,17,18,27], in particular the typical bands for phosphate (1050 cm^{-1}, ν_3) and for hydroxyl libration mode (632 cm^{-1}). As predictable, no bands corresponding to carbonate group were observed in this spectrum.

The (Ca,Ni)Hap spectrum (Fig. 5B) shows some changes when compared with stoichiometric CaHap. The ν_3 (antisymmetric stretching vibration) of the PO_4^{3-} group does not shift significantly when is compared with that of the CaHap spectrum [18]. However, by the study of the bands correspondent to the bending modes of the phosphate groups, it is possible to obtain useful information about the bond properties of these polyatomic groups. The 650–550 cm^{-1} region exhibits three features, two main bands at 603 and 564 cm^{-1} and a shoulder at 575 cm^{-1}. The first two bands were clearly assigned to ν_4 mode. The 575 cm^{-1} shoulder has been reported previously in synthetic and biological apatites and it is generally attributed to the HPO_4^{2-} ions [13,17–19,22]. The presence of HPO_4^{2-} is confirmed in this sample by the existence of an additional band at 870 cm^{-1} which is characteristic of the P–OH vibration. The ν_{OH} stretching vibration (3572 cm^{-1}) [13,25,27] and the corresponding librational mode, placed at 632 cm^{-1}, see Fig. 5A, characterize the OH^- vibrations in the pure CaHap. The corresponding values measured in the (Ca,Ni)Hap are included in Table 2. A gradual decrease in the intensity of these bands, accompanied by a slight displacement of the position of both bands towards lower wavenumbers, has been observed when metal substitution in the solid phase is increased [18].

To analyze data coming from the samples synthesized in solutions with 50% of CO_3^{2-} one need to account the places where carbonate can be incorporate in the apatite structure. According to the literature [19,22,29,32,33], the incorporation of carbonate into the apatite may take place by substitution for hydroxyl (type A) or for phosphate group (type B). The characteristic bands of carbonate occur in the spectra region 1590–1400 cm^{-1} (antisymmetric stretching, ν_3, strong and wide); 870–880 cm^{-1} (out-of-plane bending $\pi(CO_3)$, ν_2, medium,

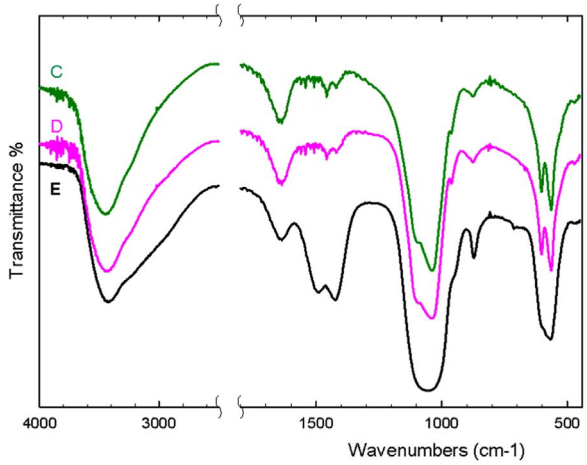

Fig. 4. FTIR spectra of nickel carbonate apatite synthesized at different temperatures: C) $NiCO_3h5_{25}$ D) $NiCO_3h5_{37}$, E) $NiCO_3h5_{100}$.

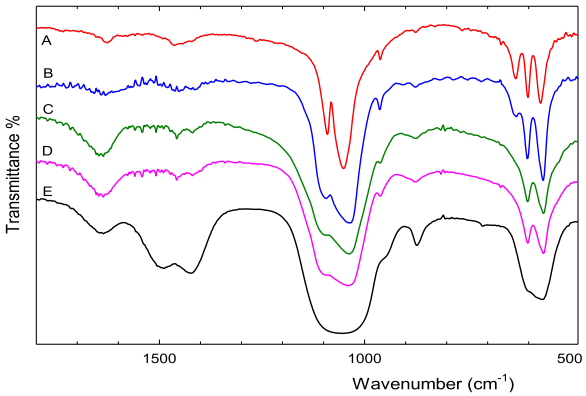

Fig. 5. FTIR spectra of different samples; calcium hydroxyapatite with different percent of nickel in solution: A) CaHap (Ni(II): 0%) and B) (Ca,Ni)Hap (Ni(II): 5%) [27]. Samples synthesized from solutions with 5% of Ni(II) and 50% of CO_3^{2-} at different temperatures: C) $NiCO_3h5_{25}$ (25 °C), D) $NiCO_3h5_{37}$ (37 °C), E) $NiCO_3h5_{100}$ (100 °C).

Table 2
Band assignment for apatitic compounds with different concentration of nickel in the solid phase.

Sample*	% of Ni	ν_3 (PO_4^{3-})	ν_4 (PO_4^{3-})	ν_2 (PO_4^{3-})	ν (OH^-)	ν_2 (CO_3^{2-})	ν_3 (CO_3^{2-})
CaHap**	–	1084, 1045	601, 572	474	3572		–
(Ca,Ni)Hap	1.1 (1)+	1097,1035	603, 575(sh) 564	476	3568		–
$NiCO_3h5_{25}$	2.2 (1)	1100, 1042	602; 572(w) 564	471 (w)	3568 (w)	880,876	1570(vw),1542 (vw),1506(vw), 1465,1460,1448, 1419
$NiCO_3h5_{37}$	2.1 (1)	1100, 1042	602;572(w) 564	471 (w)	3568 (w)	880,876	1570(vw),1542 (vw),1506(vw), 1465,1460,1448, 1419
$NiCO_3h5_{100}$	3.2 (1)	1058	602 (w), 566	471 (vw)	–	873,[ν_4:712(w)]	1506(s),1488, 1423(s),

*All the nickel containing samples were synthesized in presence of 5% of this ion in solution.
s: strong, w- weak, vw: very weak, sh: shoulder.
+data obtained from sample synthesized as shown in Ref. [18].
**data obtained from sample synthesized as shown in Ref. [27] and references therein.

sharp) and ~ 700 cm^{-1} δ(OCO) (medium-weak, ν_4, sharp) [13,22,32,33]. In the earlier studies on natural and synthetic apatites, it was found that type A was characterized by a doublet band at about 1545 and 1450 cm^{-1} (ν_3) and a singlet band at about 878 cm^{-1} (ν_2), where type B carbonate has these bands at about 1455, 1410 and 871 cm^{-1}, respectively [13,23,24,35]. At the beginning of the 21st century, I. R. Gibson and M. E. Fleet demonstrated that the presence of additional bands at the region of 1600–1400 cm^{-1} and a doublet at 880 cm^{-1} indicated the formation of type AB apatites [23,24].

For the $NiCO_3h5_{25}$ and $NiCO_3h5_{37}$ samples, carbonate bands were observed for ν_3 mode at approximately 1560, 1542, 1507, 1473, 1458 and 1419 cm^{-1} and for the ν_2 at 880 and 875 cm^{-1}. Both ν_3 and ν_2 band profiles resembled those illustrated for other type of AB carbonate apatite (AB CO_3Aps) with low carbonate content [23,24]. By contrast, $NiCO_3h5_{100}$ spectrum shows absorption characteristic of type B CO_3^{2-} substitution with substantial carbonate content: ν_3 CO_3^{2-} bands at 1420 and 1485 cm^{-1} and a ν_2 CO_3^{2-} at 873 cm^{-1}. Both ν_3 and ν_2 band intensities and positions would indicate a type B apatite with high carbonate incorporation. However, the presence of the 712 cm^{-1} band for the ν_4 mode (see Fig. 4) suggests the formation of an AB CO_3Aps with a low site A occupation.

The Ni(II)/CO_3^{2-} co-substitution did not appear to affect significantly the phosphate band positions (Table 2). However, it should be noted that the relative intensity of the hydroxyl stretching band in $NiCO_3h5_{25}$ and $NiCO_3h5_{37}$ at 3568 cm^{-1} was lower than that of the hydroxyl band in (Ca,Ni)Hap and that the OH^- librational band (around 630 cm^{-1}) is absent. While in the $NiCO_3h5_{100}$ spectrum both bands are not detected. A similar intensity decrease of the hydroxyl bands at 3572 and 630 cm^{-1} in samples with Mg(II)/CO_3^{2-} co-substitution was observed from FTIR data by Gibson and W. Bonfield [23].

3.2.2. X-ray diffraction results

The XRPD patterns of carbonate apatite phases synthesized with 5% of Ni (II) and 50% of CO_3^{2-} ions at 25, 37 and 100 °C are shown in Fig. 6. No lines of brushite or monetite phases could be detected in these patterns. The analysis of data obtained for the samples synthesized at the lower temperatures (25 and 37 °C) showed coexistence of two phases: one, with well defined lines in $NiCO_3h5_{25}$ sample, could be identified as $CaCO_3$ [37] and the second, which exhibit broad and not well defined lines, as carbonate apatite [25]. Intensity and crystallinity of $CaCO_3$ phase diminish as temperature of synthesis increases as can be seen in sample $NiCO_3h5_{37}$. No $CaCO_3$ lines could be recognized in sample $NiCO_3h5_{100}$.

3.2.3. SEM images

The SEM images of $NiCO_3h5_{37}$ sample, Fig. 7A and B, presenting different image magnification, showed smaller grain size than that of $NiCO_3l5$. No clear crystalline planes could be detected from these

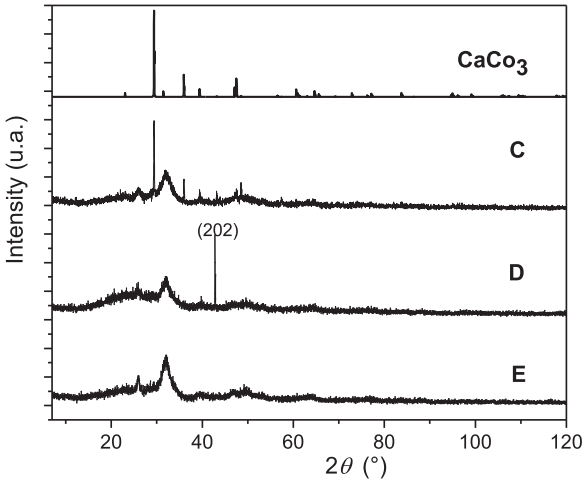

Fig. 6. X-ray diffraction patterns of the carbonate apatite phases synthesized with 5% percentage of Ni (II) and 50% of CO_3^- ions at different temperatures: C) $NiCO_3h5_{25}$ (25 °C); D) $NiCO_3h5_{37}$, (37 °C), and E) $NiCO_3h5_{100}$ (100 °C). Lines of $CaCO_3$ are included for comparison.

images, which resemble those coming from cortical bone carbonate apatite, as seen in Fig. 8, where an image obtained from bovine cortical bone thermally treated at 400 °C is exposed for comparison. Difference in crystallite sizes in brushite and other Ca-P phases present in kidney stones has been observed by Daudon et al. [38,39], who found out (in kidney stone SEM studies) that with exception of brushite, which forms large crystals, all other phases of calcium phosphates form tiny particles made of nanocrystals less than 15 nm in size.

4. Discussion

Studies of the apatite phase formation in aqueous systems are important because of their direct relevance to biological mineralization [12,13,17]. Apatite formation generally occurs through one or more unstable intermediates which subsequently transform to thermodynamically stable phases [12,13,15,17,22].

From the present study results, it is found out that, when the levels of carbonate are high, a carbonate apatite phase is formed. A common method for determining the type of carbonate substitution in CaHap is the study of the positions of carbonate bands in the FTIR spectra [13,18,22–25,29,32–36,42,43].

Carbonate apatite, as the main mineral components of the vertebrate´s bone and teeth, has drawn substantial attention not only from mineralogical but also from biological points of view [13,14,22,27]. It is generally agreed that the carbonate ion can be a substitute for OH^- in the apatite channel (type A) or for the phosphate ion (type B). Type A substitution tends to increase lattice parameter *a*, but to decrease *c*,

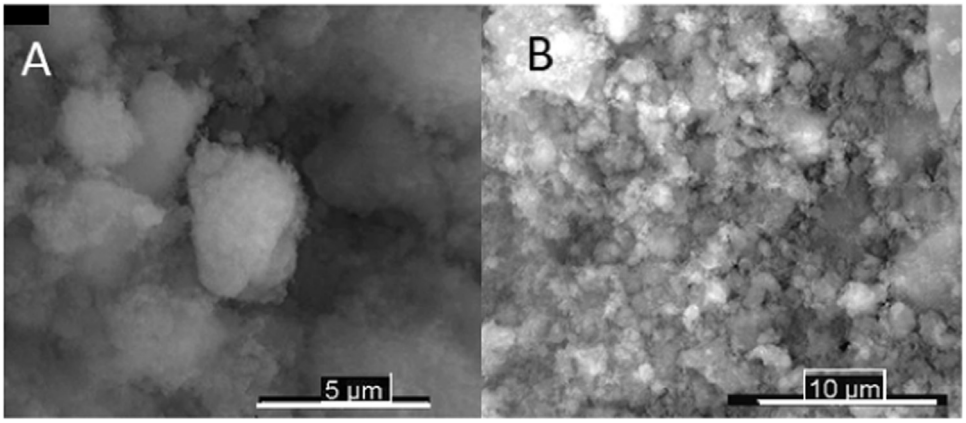

Fig. 7. SEM image of $NiCO_3h_{37}$ crystallites. Scales: A) 5 µm; B) 10 µm.

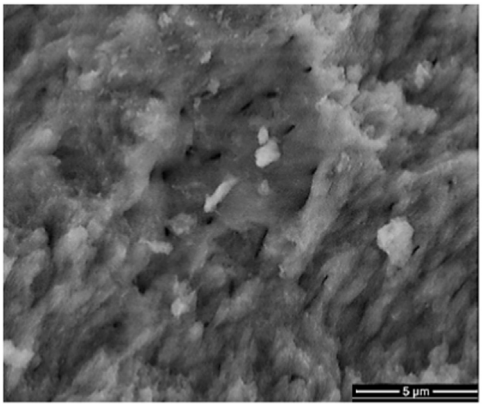

Fig. 8. SEM image of bovine cortical bone thermally treated at 400 °C.

whereas type B substitution induces the opposite effect [22,32]. These two different structural substitutions create lattice distortions, microstresses and crystal defects affecting the biological behavior of apatite graft material, particularly through the enhanced osteointegration ability [13,14,22,23].

However, recent studies have indicated that a more stable substitution is type AB in which two carbonate ions replace one phosphate group and one hydroxyl group, respectively [43]. The $(Ca,Ni)CO_3Ap$ prepared at 25 and 37 °C in this study present carbonate bands at 1570, 1542, 1507, 1473, 1458, 1419 cm^{-1} for the ν_3, at 880 and 873 cm^{-1} for the ν_2 band, and at 712 cm^{-1} for the ν_4 band. The values obtained for the ν_3 bands were compared satisfactorily to those obtained by Gibson et al. [23], thus indicating carbonate substitution in both positions. Further evidence of substitution of carbonate in both positions is the doublet peak observed for the carbonate ν_4 bands at 880 and 873 cm^{-1}. It should be noted that the absence of bands at 880 cm^{-1} in the sample $NiCO_3h5_{100}$ could put in doubt the formation of an AB CO_3Aps in this sample. However, the presence of weak bands at 755 and 675 cm^{-1} evidence, as M. Vignoles et al. [42] have described, some type A carbonate substitution in the structure. For that reason, we consider the absence of bands in 880 cm^{-1} as evidence that there was a greater level of carbonate substitution on the phosphate B site than on the hydroxyl site for this sample. Further support to these preferential substitutions is the difference of the band intensities at 1489 cm^{-1} (corresponding to A substitutions) and 1422 cm^{-1}.

In general, the phosphate bands positions found in $(Ca,Ni)CO_3Ap$ did not differ significantly from the values observed in (Ca,Ni)Hap (see Table 2, for a broader discussion of bands see reference 18). However, the doublet correspondent to the PO_4^{3-} ν_2 band at 473 and 448 cm^{-1} was observed for $(Ca,Ni)CO_3Ap$, whereas only a single peak was observed for (Ca,Ni)Hap at 476 cm^{-1}, which was an additional indication of carbonate substitution in B site.

The very weak bands attributed to hydroxyl group were observed at 3568 cm^{-1} for $NiCO_3h5_{25}$ and $NiCO_3h5_{37}$ samples, but no for $NiCO_3h5_{100}$ (see Fig. 5C and D). The decrease in intensity of these bands is due to the incorporation of nickel and carbonate into the apatite phase. Both ions provoke an increase of absorption of water in the structure, helping hydrogen bond linking between OH^- and H_2O.

In previous work, we have put in evidence that the partial Ca(II) substitution by Ni(II) [18] produces a reduction in the crystallinity degree, a shrinking in lattice parameters and a decrease in thermal stability of the synthesized (Ca,Ni)Hap.

The CaHap crystal structure shows two inequivalent Ca(II) sites. Cations at site **I**, **CaI**, are coordinated by nine oxygens belonging to six PO_4^{3-} forming triangles and displaying a columnar arrangement [13,18,27,43], while cations at site **II, CaII,** exhibited coordination seven. Six of the oxygen atoms belong to five PO_4^{3-} anions and the seventh position is occupied by an OH^- anion. Structure analysis also reveals that the smallest distances between a cation and a coordinated oxygen is at site **II**, while the smallest Ca–Ca distances are observed between Ca(II) ions at site **I**. This result together with data obtained in the present work back the hypothesis of Ca(II) substitution for Ni (II) in site II in stoichiometric CaHap, in contrast to the observed Ca(II) replacement by Mg(II) in CaHap (only in Ca(I) site) [18].

This assumption is mainly supported by the remarkable changes observed in OH^- bands, which belong to the coordination sphere of Ca(II) ions at site **II**. The substitution of Ca(II) by a smaller cation like Ni(II) at this site allowed the replacement of OH^- ions by water (or the bond of water to it). This process could explain the changes observed in the infrared spectra and may induce a loss of the crystallinity that increases with the Ni(II) content [13,18].

As was discussed above, the carbonate bands observed in the spectra of $(Ca,Ni)CO_3Ap$ samples indicate that carbonate ions have substituted some PO_4^{3-} and OH^- ions in the apatite lattice (type AB substitution). A.A. results evidence an increased incorporation of Ni(II) in these samples when compared with (Ca,Ni)Hap samples (see Table 2). However, the percentage of Ni(II) incorporated in the solid was lower than expected according to the initial nickel concentration in solution. This generates a deficiency of charge that should be compensated by other ions or vacancies.

Previous experimental and theoretical studies on biological and synthetic apatites have identified carbonate groups located in the positions of hydroxyl ions and/or phosphate groups [22,37,43]. Based on these results and other obtained in the studies of (Ca,Ni) Hap [18], three models of possible charge compensation mechanisms were considered:

1. The partial substitution of Ca(II) by Ni(II), introducing a Ca(II) ion (V_{Ca}) and an OH^- ion vacancy (V_{OH}) [18].

$Ca_{10}(PO_4)_6(OH)_2 + Ni^{2+} \rightarrow (Ca,Ni)_{10-x}(V_{Ca})_x(PO_4)_6(OH)(V_{OH})_{2\times} + 2x\ OH^- + x\ Ca^{2+} + Ca^{2+}$.

2. Type B substitution, introducing a Ca(II) ion (V_{Ca}) and an OH^- ion vacancy (V_{OH}) [43].

$Ca_{10}(PO_4)_6(OH)_2 + CO_3^{2-} \rightarrow (Ca)_9(V_{Ca})(PO_4)_5(CO_3)(OH)(V_{OH}) + PO_4^{3-} + OH^- + Ca^{2+}$.

3. Type AB substitution, where a PO_4^{3-} and an OH^- were replace by two CO_3^{2-} [43].

$Ca_{10}(PO_4)_6(OH)_2 + 2\ CO_3^{2-} \rightarrow (Ca)_{10}(PO_4)_5(CO_3)_2(OH) + PO_4^{3-} + OH^-$.

Considering all these aspects, we assume that the positively charged vacancies (generated by the percentage of Ni(II) incorporated lower than 100%) were compensated by the incorporation of CO_3^{2-} instead of PO_4^{3-} and OH^-, as represented by the following reaction:

$Ca_{10}(PO_4)_6(OH)_2 + 2\ CO_3^{2-} + Ni^{2+} \rightarrow (Ca,Ni)_9(V_{Ca})(PO_4)_5(CO_3)_2(OH)(V_{OH}) + PO_4^{3-} + OH^- + Ca^{2+}$.

Consequently, holes in the structure give rise to the incorporation of H_2O in the solid. This interpretation is consistent with the water band intensity increase (3452 and 1650 cm^{-1}) and with bands broadening in the region 1100–1000 ($\upsilon_3\ PO_4^{3-}$) and around the 565 cm^{-1} ($\upsilon_4\ PO_4^{3-}$) line. Indeed the broad lines observed in the (Ca,Ni)CO_3Ap phase present in the X-ray patterns of $NiCO_3h5_x$, is an evidence of incorporation of water in the structure.

Current report reveals that, when nickel and carbonate ions are simultaneously present in solution, they are incorporated in the apatite phase only when there are high carbonate level. The inclusion of carbonate causes an increase in nickel incorporation (Table 2), while the presence of nickel did not have a significant effect on the incorporation of carbonate. However, when the level of carbonate ion decreases and its proportion became similar to that of the nickel ion, the later has an inhibiting effect on the apatite formation.

Recalling our previous and present results and others found in the literature, it can be stated that the hydroxyapatite is preferentially formed under neutral or basic conditions, but, in more acidic solutions (pH 6.5–6.8), other phases, like brushite, are often found [12,13,16,17]. Brushite has been implicated as possible precursor to the formation of apatite [12,13,17,19,40,41]. It has been often detected during in vitro crystallization, but it has not been frequently found in biological systems [12,13]. However, as described in the introduction and in our recent work [16], brushite has been increasingly found as part of kidney stones formation, being and apparent cause of stones promotion and recurrence [1–3,16]. According to present analysis, when both ions (Ni^{2+} and CO_3^{2-}) are in similar concentrations (5%), at pH 7 and temperatures 25 or 37 °C, the transformation of brushite to CaHap does not occur. Under these conditions, and in absence of nickel, the formation of hydroxyapatite phase generally takes place. Besides, as shown, in a previous study [16], the presence of low levels of nickel stabilizes the brushite phase and prevent it from converting to apatite.

On the other hand, when the carbonate concentration is considerably higher than the nickel concentration in solution, the apatite phase precipitates as it was observed in the $NiCO_3h5_x$ samples. The same principles may control the urinary stones development [9]. This would explain the low incidence of brushite stones in renal pathologies [7–9,14–16,40]. Its advent to the kidney stone scenario in the last decades would suggest an appearance of Ni(II) in the biological fluid and/or a metabolic problem, which reduces the presence of carbonate in biological fluid.

5. Conclusions

The previous work results coming from FTIR spectroscopy, X-ray powder diffraction and chemical analysis confirm the synthesis of brushite at 25 °C (and 37 °C) and neutral pH when different amounts of Ni(II) as doping element are included in phosphate synthesis. The present investigation demonstrates that those results are persistent at the presence of small levels of carbonate among reaction products.

When the preparations were done in the presence of low levels of Ni(II) and high levels of carbonate, three (Ca,Ni)CO_3Ap were synthesized as a function of synthesis temperature. FTIR analysis detected carbonation in both positions, A and B, for all apatite products. The maximum carbonation obtained by this method was found in the samples synthesized at 100 °C. Chemical analysis evidenced an increase of CO_3^{2-} substituting for PO_4^{3-} in the apatite lattice in $NiCO_3h5_{100}$.

The obtained results might have some possible biological implications as they suggest that brushite kidney stones may develop as a result of a decrease in the levels of carbonate and the simultaneous presence of Ni (II) traces in biological fluids.

Acknowledgements

The authors acknowledge National Scientific and Technological Research Council of Argentina (CONICET) projects: PIP 0651, PIP 0327 and PIP 0359; Universidad Nacional de La Plata (UNLP, Argentina) projects: 11X565, 11X672 and 11X709, Departamento de Ciencias Básicas de la Universidad Nacional de Luján (UNLu, Argentina) projects B112 and B152, SNRX (MINCyT) and CONICET (Joint Projects RXAC7 and RXM8) for financial support. J.A.G and G.P. are members of the CONICET research staff.

References

[1] F.L. Coe, E.M. Worcester, A.P. Evan, Idiopathic hypercalciuria and formation of calcium renal stones, Nat. Rev. Nephrol. 12 (2016) 519–533 (and references therein).
[2] J. Cloutier, L. Villa, O. Traxer, M. Daudon, Kidney stone analysis: “give me your stone, I will tell you who you are!”, World J. Urol. 33 (2015) 157–169. http://dx.doi.org/10.1007/s00345-014-1444-9.
[3] L. Borghi, T. Schianchi, T. Meschi, A. Guerra, F. Allegri, U. Maggiore, A. Novarini, Comparison of two diets for the prevention of recurrent stones in idiopathic hypercalciuria, N. Engl. J. Med. 346 (2002) 77–84.
[4] E.N. Taylor, G.C. Curhan, Fructose consumption and the risk of kidney stones, Kidney Int. 73 (2008) 207–212.
[5] A.E. Krambeck, S.E. Handa, A.P. Evan, J.E. Lingeman, Profile of the brushite stone former, J. Urol. 184 (2010) 1367–1371.
[6] S.R. Khan, B.K. Canales, A unified theory on the pathogenesis of randall's plaques and plugs, Urolithiasis 43 (2015) 109–123. http://dx.doi.org/10.1007/s00240-014-0705.
[7] A.P. Evan, J.E. Lingeman, E.M. Worcester, Contrasting histopathology and crystal deposits in kidneys of idiopathic stone formers who produce hydroxyapatite, brushite, or calcium oxalate stones, Anat. Rec. 297 (2014) 731–736.
[8] A.E. Krambeck, S.E. Handa, A.P. Evan, et al., Profile of the brushite stone former, J. Urol. 184 (2010) 11.
[9] L. Shiyan, Z. Wenjun, W. Lijun, Direct nanoscale imaging of calcium oxalate crystallization on brushite reveals the mechanisms underlying stone formation cryst, Growth Des. 15 (2015) 3038–3045.
[10] N.S. Mandel, I.C. Mandel, A.M. Kolbach-Mandel, Accurate stone analysis: the impact on disease diagnosis and treatment, Urolithiasis 45 (2017) 3–9. http://dx.doi.org/10.1007/s00240-016-0943.
[11] J.C. Williams Jr, E. Worcester, J.E. Lingeman, What can the microstructure of stones tell us?, Urolithiasis 45 (2017) 19–25.
[12] J. Guerra-López, J.A. Güida, C.O. Della Védova, Infrared and Raman studies on renal stones: the use of Second derivative infrared spectra, Urol. Res. 38 (2010) 383–390.
[13] J.R. Guerra-López García, Tesis Doctoral, Universidad Nacional de Luján and references therein, 2005.
[14] J.R. Guerra-López García, J.A. Güida, Aplicación de la espectroscopia IR en el estudio de la composición de cálculos renales, Editorial Académica Española, Saarbrücken, Germany, 2012.
[15] D. Bazin, M. Daudon, C. Combes, C. Rey, Characterization and some physico-chemical aspects of pathological microcalcifications, Chem. Rev. 113 (2012) 5092–5120.
[16] J.R. Guerra-López, J.A. Güida, M.A. Ramos, G. Punte, The influence of nickel on brushite structure stabilization, J. Mol. Struct. 1137 (2017) 720–724.
[17] J. Guerra-López, R. González, A. Gómez, R. Pomés, G. Punte, C.O. Della Védova, Effects of nickel on calcium phosphate formation, J. Solid State Chem. 151 (2000) 163–169.
[18] J. Guerra-López, R. Pomés, C.O. Della Védova, R. Viña, G. Punte, Influence of nickel on hydroxyapatite crystallization, J. Raman Spectrosc. 32 (2001) 255–261.
[19] R.Z. LeGeros, Calcium phosphates in oral biology and medicine, in: H.M. Myers

(Ed.), Monographs in Oral Sciences 15, Karger, Basel, 1991.
[20] T. Lee, Y.C. Lin, Mimicking the initial development of calcium urolithiasis by screening calcium oxalate and calcium phosphate phases in various urinelike solutions, time points, and pH values at 37 °C, Cryst. Growth Des. 11 (2011) 2973–2992.
[21] M. Rui-hong, L. Xiao-bing, Q. Li, Z. Hai-qiang, The systematic classification of urinary stones combine-using FTIR and SEM-EDAX, Inter. J. Surg. 41 (2017) 150–161.
[22] J.C. Elliot, Structure and Chemistry of Apaptites and Other Calcium Othophosphates, Elsevier, Amsterdam, London, New York, Tokyo, 1994.
[23] I.R. Gibson, W. Bonfield, Novel synthesis and characterization of an AB-type carbonate-substituted hydroxyapatite, J. Biomed. Mater. Res. 15 (59) (2002) 697–708.
[24] M.E. Fleet, X. Liu, Location of type B carbonate ion in type A–B carbonate apatite synthesized at high pressure, J. Solid State Chem. 177 (2004) 3174–3182.
[25] R.M. Wilson, S.E.P. Dowker, J.C. Elliott, Rietveld refinements and spectroscopic structural studies of a Na-free carbonate apatite made by hydrolysis of monetite, Biomaterials 27 (2006) 4682–4692.
[26] A. Tovborg-Jensen, J. Rathlev, Vibration spectra of brushite, $CaHPO_4 \cdot H_2O$, Inorg. Syn. 4 (1953) 19–24.
[27] J.R. Guerra-López, G.A. Echeverría, J.A. Güida, R. Viña, G. Punte, Synthetic hydroxiapatites doped with Zn(II) studied by X-ray diffraction, infrared, Raman and thermal analysis, J. Phys. Chem. Solids 81 (2015) 57–65.
[28] G.J. Bates, Res. Natl. Bur. Std. (Us) 66 a (1999) 179.
[29] R.Z. LeGeros, R. Kijkowska, C. Bautista, J.P. LeGeros, Synergistic effects of magnesium and carbonate on properties of biological and synthetic apatites, Conn. Tiss. Res. 33 (1995) 203–207.
[30] N.A. Curry, D.W. Jones, Crystal structure of brushite, calcium hydrogen orthophosphate dihydrate: a neutron-diffraction investigation, J. Chem. Soc. A (1971) 3725–3729.
[31] M. Catti, G. Ferraris, A. Filhol, Hydrogen bonding in the crystalline state. $CaHPO_4$ (monetite), P–1 or P1. A novel neutron diffraction study, Acta Crystallogr. Sect. B 33 (1977) 1223–1229.
[32] J.C. Labarthe, G. Bonel, G. Montel, Sur la structure et les propriétés des apatites carbonatées type B phosphocalciques, Ann. Chim. 8 (1973) 289–301 (14th Series).
[33] R.Z. LeGeros, J.P. LeGeros, O.R. Trautz, E. Klein, Spectral properties of carbonate in carbonate-containing apatites, Dev. Appl. Spectrosc. 7B (3) (1970) 3–12.
[34] C. Rey, B. Collins, T. Goehl, I.R. Dickson, M.J. Glimcher, The carbonate environment in bone mineral: a resolution-enhanced Fourier Transform Infrared Spectroscopy Study, Calcif. Tissue Int. 45 (1989) 157–164.
[35] E.A.P. De Maeyer, R.M.H. Verbeeck, D.E. Naessens, Optimalization of the preparation of Na^+-containing and CO_3^{2-}-containing hydroxyapatite by the hydrolysis of monetite, J. Cryst. Growth 135 (1994) 539–547.
[36] M.E. Fleet, X. Liu, Carbonate apatite type A synthesized at high pressure: new space group (P3) and orientation of channel carbonate ion, J. Solid State Chem. 174 (2003) 412–417.
[37] E.N. Maslen, V.A. Streltsov, N.R. Streltsovova, X-ray study of the electron density in calcite CaCO3, Acta Cryst. B49 (1993) 636–641.
[38] M. Daudon, O. Traxer, P. Jungers, A.P. Evan, J.E. Lingeman, J.C. Williams Jr. (Eds.), Renal Stone Disease, Am. Instit. Physics Conf. Proceedings, Melville, 900, 2007, p. 26.
[39] M. Daudon, A. Dessombz, V. Frochot, E. Letavernier, J.P. Haymann, P. Jungers, D. Bazin, Comprehensive morpho-constitutional analysis of urinary stones improves etiological diagnosis and therapeutic strategy of nephrolithiasis, C. R. Chim. 19 (2016) 1470–1491.
[40] A. Hesse, D. Heimbach, Causes of phosphate stone formation and importance of metaphylaxis by urinary acidification: a review, World J. Urol. 17 (1999) 308–3015.
[41] H.E. Lundager Madsen, Influence of foreign metal ions on crystal growth and morphology of brushite ($CaHPO_4$, $2H_2O$) and its transformation to octacalcium phosphate and apatite, J. Cryst. Growth 310 (2008) 2602–2612.
[42] M. Vignoles, G. Bonel, R.A. Young, Occurrence of nitrogenous species in precipitated B-type carbonated hydroxyapatites, Calcif. Tissue Int. 40 (1987) 64–70.
[43] F. Ren, X. Lu, Y. Leng, Ab initio simulation on the crystal structure and elastic properties of carbonate apatite, J. Mech. Behav. Biomed. Mater. 26 (2013) 59–67.